Naval Research Laboratory
Washington, DC 20375-5320

NRL/6730/MR—2024/1

Green Stimulated Rotational Raman Scattering for Utilization in Laser Inertial Confinement Fusion Reactor

DR. MATTHEW F. WOLFORD

T. JUDE KESSLER

ERNESTO BARRAZA-VALDEZ

Laser Plasma Branch
Plasma Physics Division

STEPHEN P. OBENSCHAIN

Laser Fusion X
Springfield, VA

March 6, 2024

REPORT DOCUMENTATION PAGE

PLEASE DO NOT RETURN YOUR FORM TO THE ABOVE ORGANIZATION

1. REPORT DATE	2. REPORT TYPE	3. DATES COVERED	
06-03-2024	NRL Memorandum Report	START DATE 10/01/2020	END DATE 09/30/2023

4. TITLE AND SUBTITLE
Green Stimulated Rotational Raman Scattering for Utilization in Laser Inertial Confinement Fusion Reactor

5a. CONTRACT NUMBER	5b. GRANT NUMBER	5c. PROGRAM ELEMENT NUMBER
5d. PROJECT NUMBER	**5e. TASK NUMBER**	**5f. WORK UNIT NUMBER**
		9387

6. AUTHOR(S)
Dr. Matthew F. Wolford, T. Jude Kessler, Ernesto Barraza-Valdez, and Stephen P. Obenschain*

7. PERFORMING ORGANIZATION / AFFILIATION NAME(S) AND ADDRESS(ES)
Naval Research Laboratory
4555 Overlook Ave SW
Washington, DC 20375-5320

8. PERFORMING ORGANIZATION REPORT NUMBER
NRL/6730/MR—2024/1

9. SPONSORING / MONITORING AGENCY NAME(S) AND ADDRESS(ES)	10. SPONSOR / MONITOR'S ACRONYM(S) NUMBER	11. SPONSOR / MONITOR'S REPORT NUMBER(S)
National Nuclear Security Administration Department of Energy 1000 Independence Ave SW, Washington, DC 20375	DOE	

12. DISTRIBUTION / AVAILABILITY STATEMENT
DISTRIBUTION STATEMENT A: Approved for public release; distribution is unlimited.

13. SUPPLEMENTAL NOTES
*Laser Fusion X 7520 Hamlet Street, Springfield, VA 22151

14. ABSTRACT
The The U.S. Naval Research Laboratory has developed a method to change the laser spectral width from a very narrow frequency bandwidth ~3 GHZ at full width half maximum to a range of at least 17 THZ in frequency bandwidth utilizing a stimulated rotational Raman scattering process (SRRS). The greater than 3 orders of magnitude (5000 times) in spectral range was achieved utilizing propagation in air and taking advantage of the SRRS response of nitrogen and oxygen. The SRRS process can be enhanced in focal geometry utilizing elliptical (circular) polarization relative to linear polarization. Seeding higher frequency Raman (anti-Stokes) transitions of air diatomic molecules can generate measurable light at equivalent lower frequency Raman (Stokes) transitions. The ability to increase bandwidth for solid state lasers utilizing an inexpensive medium such as air offers potential to be utilized in laser fusion ignition scale facilities to mitigate laser plasma instabilities. Mitigation of laser plasma instabilities (LPI) in a controlled manner offers the opportunity to control the spatial laser power with interaction of multiple laser beams as well as allow higher coupling (more energy) to various targets that otherwise would be limited without significant laser modification.

15. SUBJECT TERMS

16. SECURITY CLASSIFICATION OF:			17. LIMITATION OF ABSTRACT	18. NUMBER OF PAGES
a. REPORT	b. ABSTRACT	c. THIS PAGE		
U	U	U	SAR	27

19a. NAME OF RESPONSIBLE PERSON	19b. PHONE NUMBER *(Include area code)*
Dr. Matthew Wolford	(202) 767-3528

This page intentionally left blank.

CONTENTS

FIGURES

(the list of figures is optional)

TABLES

(the list of tables is optional)

EXECUTIVE SUMMARY

The U.S. Naval Research Laboratory has developed a method to change the laser spectral width from a very narrow frequency bandwidth ~3 GHZ at full width half maximum to a range of at least 17 THZ in frequency bandwidth utilizing a stimulated rotational Raman scattering process (SRRS). The greater than 3 orders of magnitude (5000 times) in spectral range was achieved utilizing propagation in air and taking advantage of the SRRS response of nitrogen and oxygen. The SRRS process can be enhanced in focal geometry utilizing elliptical (circular) polarization relative to linear polarization. Seeding higher frequency Raman (anti-Stokes) transitions of air diatomic molecules can generate measurable light at equivalent lower frequency Raman (Stokes) transitions. The ability to increase bandwidth for solid state lasers utilizing an inexpensive medium such as air offers potential to be utilized in laser fusion ignition scale facilities to mitigate laser plasma instabilities. Mitigation of laser plasma instabilities (LPI) in a controlled manner offers the opportunity to control the spatial laser power with interaction of multiple laser beams as well as allow higher coupling (more energy) to various targets that otherwise would be limited without significant laser modification.

This report presents research conducted by the Laser Plasma Branch in the Plasma Physics Division including Dr. Matthew F. Wolford (Code 6733), Mr. Jude Kessler (Code 6733), Mr. Ernesto Barraza-Valdez (Code 6733) and Dr. Stephen P. Obenschain (Laser Fusion X and formerly Code 6730, now retired).

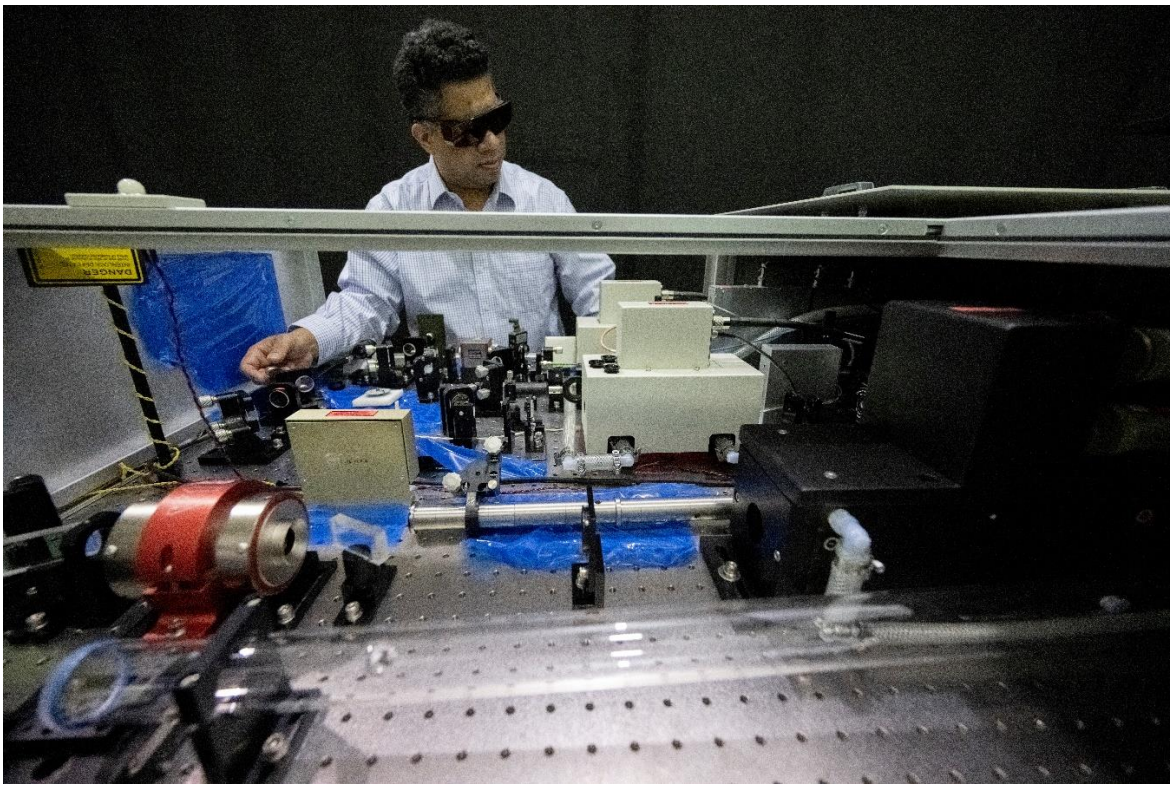

Fig. E1 — Mr. Jude Kessler operating the 10 J Green Nd:Glass Laser

This page intentionally left blank.

GREEN STIMULATED ROTATIONAL RAMAN SCATTERING FOR UTILIZATION IN LASER INERTIAL CONFINEMENT FUSION REACTOR

1. INTRODUCTION

NRL has made progress in generating broad bandwidths utilizing SRRS in air with a modest Nd:Glass green laser. Stimulated Rotational Raman Scattering is a process of generating broad bandwidth light utilizing diatomic molecules such as oxygen and nitrogen, the components of air. The applicable concept for inertial confinement fusion is to use modern ignition scale laser systems (i.e. NIF) of today and add bandwidth by propagating through inexpensive media, air, with very few additional optics. NRL is investigating the feasibility of this approach with a 10 J green laser which has a controllable 1-6 ns pulseshape. NRL has initially examined a method by focusing the laser light in air, which is similar concept of D. Eimerl work at LLNL [1], to generate the initial seed. One approach is to use a portion of the ICF laser facility beam line through a focal geometry to generate the broadband light seed and co-propagate with the remaining laser energy of the large scale ICF laser facility beam lines. Our initial thought is to utilize green wavelengths to allow utilization of much higher energies (intensities) to mitigate laser plasma instabilities and reach the desired target. The generated light composed of the anti-Stokes shorter wavelengths and high frequencies, the pump (initial laser wavelength) and Stokes lines which are generated at longer wavelengths or smaller frequencies. The Stokes wavelength generation can occur with multiple orders depending on conditions of the laser pulses utilized and the SRRS media characteristics. The generated light is at discrete frequencies corresponding to the allowed rotational Raman transitions for the homonuclear diatomic molecules (N_2 & O_2) at integers of the Rotational Constant (B) and accounting for the minor effect of the Centrifugal Distortion Constant (D).

The use of a second laser is an alternative method of generating the SRRS seed for the broadband light to target. Using a second laser pulse allows control of the broadened laser light as well as substantial bandwidth generation over shorter path lengths than unseeded. NRL is utilizing a narrow band dye laser to make SRRS measurements for seeded case in both focal geometries and collinear geometries. In addition to the importance of laser seed intensity and geometry other outstanding aspects of SRRS generation. One aspect is the laser beam modulation as the laser beam propagates to verify the laser beam does not add modulation which could pose risk to downstream optics. Another aspect is the temporal envelope of the SRRS generated light to see how close it follows the pulse shape of the pump pulse and/or seed pulse which generated it. The temporal envelope could be examined with a monochrometer backed by a streak camera for temporal resolution. In addition, examination of circular polarized light seed and pump with one being clockwise and the other being counter clockwise. The opposite Right and Left handed circular light propagation shows promise should have the highest gain and reduce the path length and/or intensity requirements to allow a broader range of viable SRRS conditions to be utilized on the ICF –class facilities. NRL has recently developed theoretical tools analytical analysis as well as being able to model polarized broadband light produced by stimulated rotational Raman scattering [2,3].

1.1 SRRS Basics

Stimulated rotational Raman scattering (SRRS) is the stimulated version of the well-known nonlinear optical process of inelastic photon scattering, whereby an incident photon interacts with a material and a

Manuscript approved February 23, 2024.

resultant photon of lower or higher energy is formed. The photon shifts lower or higher energy due to the vibrational-rotational levels available from the interacting material(s). If the photon densities are high as in a Q-switched laser beam, so that there are many photons per optical mode, the process becomes stimulated. The stimulated process can also be understood as a purely classical process where light propagates though a medium whose polarizability oscillates at a natural frequency of the medium. The oscillating polarizability is proportional to the magnitude of a mechanical oscillation in the medium. An oscillating polarizability generates the lower (and sometimes the upper) optical sideband of the incident light at a rate that depends on the magnitude of the mechanical oscillation. At the same time the mechanical oscillations are amplified by the conversion of light to the sideband frequency. The lower sideband frequency is less than the pump frequency by the frequency of the mechanical oscillations of the molecule, or equivalently the frequencies of vibrational-rotational molecular transitions. The frequency shift between the incident beam and the lower or upper sideband is known as the Raman shift.

SRRS requires an energetic powerful laser (a pump) and a source of light at the lower sideband frequency (the Stokes beam). The Stokes wave is amplified by the SRRS process throughout the pump laser pulse duration and overlap between the two waves (pump and Stokes). The Stokes wave can grow to be about the same magnitude as the pump beam. If no physical source is provided, the source will be quantum noise at the Stokes frequency or the thermal population of the vibration-rotational levels of the nitrogen molecule.

SRRS in nitrogen gas is well-known in ICF studies. Nitrogen gas is present as a coolant in laser amplifiers. If nitrogen gas is also present at sufficient partial pressure in the beam-transport tubes from the laser output aperture to the target chamber vacuum windows, SRRS originating from quantum noise can occur. Energy is transferred from the (coherent and collimated) laser pulse to amplified quantum noise, which generally occupies a large solid angle and so it is not focusable on the target. This version of SRRS is therefore a parasitic process that degrades ICF experiments.

1.2 Potential Impact of Broad Bandwidth Generation for Laser Fusion

Inertial Fusion Energy (IFE) has the potential to provide energy using hydrogen isotopes as fuel and generating cost effective electricity. Inertial Confinement Fusion (ICF) is the process of generating a single fusion event in which higher yield is generated than the energy deposited in the fuel. In laser driven ICF, laser energy is deposited and ablates the fuel target's outer layer which creates pressure that compress and heat the fuel until conditions for the Lawson Criteria [4] are reached. Laser driven ICF historically can be categorized into two concepts: direct drive and indirect drive [5]. Direct drive ICF consists of multiple high-power laser beams symmetrically shining directly on a target. Indirect drive utilizes a process with lasers hit cylindrical container (hohlraum) encasing the target. The laser light impinges on to the hohlraum inner surface and converts into x-rays which interact with the target. Direct drive has the capability of transferring and coupling more laser energy to the target (4x-6x depending on wavelength [6]) and thus being more efficient. As opposed to indirect drive which has lower efficiency due to conversion from laser light to x-rays.

Direct drive lasers due to their short wavelength create an ablation plasma close to the 'quarter critical surface.' The high intensity light passes through a lower density region (corona) before reaching the ablation plasma. The lower density region at high laser intensities can be exposed to scattered light and electron plasma waves which can initiate some laser-plasma instabilities (LPI). Extensive detailed examination of laser plasma instabilities can be found elsewhere [7-8]. LPI are processes which grow due to the feedback nature of the processes strengthening the interaction waves at higher laser intensities and over longer times at high laser intensities. LPI is detrimental for maximizing the ablation pressure on a target due to the energy being moved away from the target as well as initiating high energy electrons toward the target to 'pre-heat' and expand the target before the compression shock gets to ignition. Major laser-

plasma instabilities include two-plasmon-decay (TPD), stimulated Raman scattering (SRS), and cross-beam energy transfer (CBET) [9]. In the case of TPD, laser energy is converted into two electron plasma waves with high phase velocity which keeps them stable and doesn't allow for heating of ions. Therefore in TPD significant high energy electrons can form in the inertial confinement target and disrupt performance. SRS is process in which the laser excites and grows an electron plasma wave and another electromagnetic wave of lower frequency (larger wavelength). This happens near or below the quarter critical density of the plasma. In SRS high energy electrons are generated as well as light scattered away from the target. CBET is the process in which a laser beams excite density perturbations called stimulated Brillouin scattering (SBS) in the plasma and the laser beam is refracted away from the target [10].

There are many concepts to mitigate LPI and improve laser-to-fuel coupling efficiency, such as lowering the laser wavelength (increasing the photon energy), reducing the laser spatial coherence with induced spatial incoherence, reducing the laser temporal coherence, increasing the laser bandwidth so that the intensity diminishes at specific individual frequencies which drive LPIs and temporally vary the interaction to remove a dominant plasma response [11-15].

Studies have shown that laser driver bandwidth affects the growth of LPIs with larger bandwidth causing the intensity threshold of LPIs to increase [16-18]. In this memorandum, we focus on increasing the bandwidth of a laser by using stimulated rotational Raman scattering (SRRS) of air as a way to mitigate LPIs. SRRS is a fourwave mixing process occurring with air molecules (more specifically homonuclear diatomic molecules O_2 and N_2) which then converts some of the laser beam energy to a lower frequency (stokes) or to higher frequency (anti-stokes) [19-20]. SRRS is different than SRS as the former is an interaction between laser and symmetric molecules (such as air) interacting with rotational quanta and the latter is an interaction between laser and ionized matter (plasma). SRRS has been studied in many diatomic gases such as H_2, D_2, N_2, and O_2.

SRRS has been viewed unfavorably because experiments showed it degrades the beam quality when in the saturated regime [21-22]. In 1985, Henesian et al. conducted one of the earliest SRRS experiments using the 1.053 μm Nova laser beam [21]. Lin et al. conducted both experiments and computational analysis [22]. Both experiments showed that a laser beam can evolve into stokes beams with high divergence and low beam quality due to being in saturated regime. This would give reason to mitigate SRRS in high energy solid state laser facilities. However, modern experiments in the transient regime have shown that SRRS can be used to increase the laser bandwidth to approximately 10 THz to mitigate LPIs [23]. Recent experiments and analysis on the KrF excimer laser (Nike) at NRL have shown that SRRS can be used to increase the bandwidth to approximately 5 THz at 248 nm [3, 24-25]. In these studies, the KrF laser was propagated approximately 100 m with approximately 1 GW/cm^2 with ISI and showed a widening of the bandwidth, decrease the coherence time, and little degradation of the overall beam at the focal plane in the transient regime. The National Ignition Facility (indirect drive) and the OMEGA laser at the University of Rochester Lab for Laser Energetics (LLE) use Nd:Glass lasers and have a bandwidth of approximately 0.3 and 1 THz (respectively) due to constraints on the tripled frequency conversion and optical damage. SRRS can provide a pathway to increase bandwidth up to or beyond 10 THz on these lasers along with excimer lasers. SRRS processes are under present investigation due to their complex phenomena with differences due to laser parameters on beam size and other characteristics [26]. Additionally, SRRS has been used in conjunction with vibrational stimulated Raman scattering and Kerr nonlinearity to produce a good quality laser with supercontinuum spectrum in a nitrogen filled hollow-core fiber [27].

2. EXPERIMENTAL

Due to the fact NRL has not published nor described in detail the experiments conducted to find critical parameters for SRRS at green wavelengths, a thorough description of what was done will be here. In addition, we will discuss experiments and diagnostics which were not fully investigated/utilized. An

account of experimental challenges will also be mentioned. The sections will be the Laser representing the two utilized for the green SRRS experiments, including the high energy pump laser (Continuum Project # 17/14979) and 355 nm Nd:YAG pumped dye laser system. The other key experimental components are the Optical Layout for the experimental deployment used in the research and the Diagnostics to examine the measurement capability and utilization.

2.1 Laser

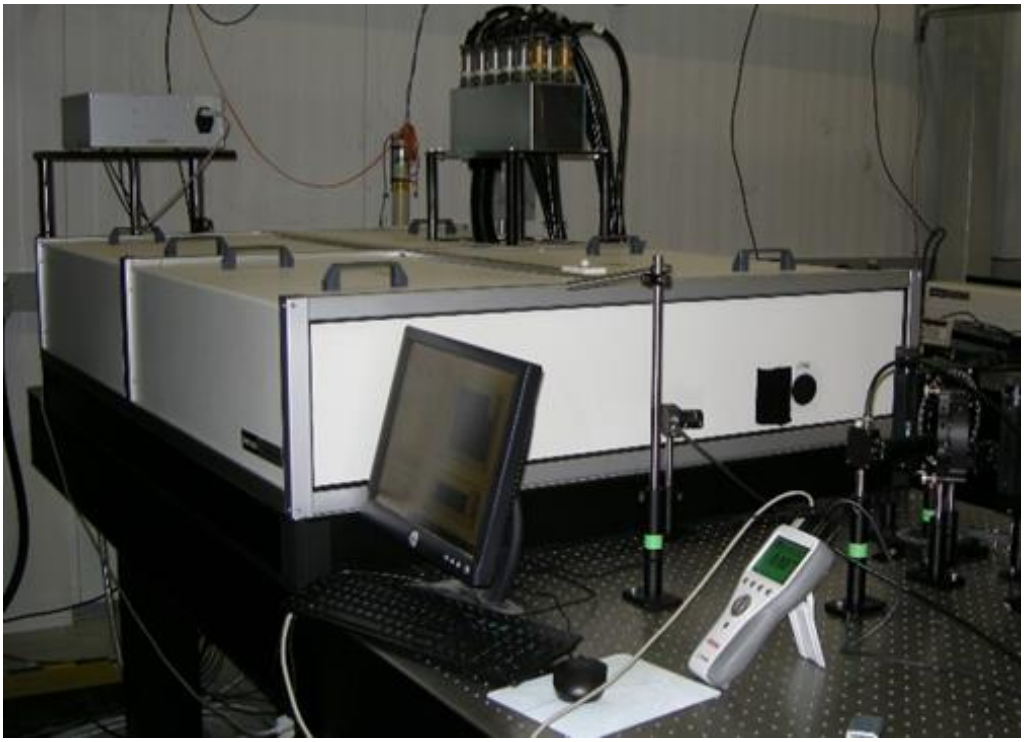

Figure 1. Exterior view of the 10 Joule, 527 nanometer, 3 nanosecond high energy pump laser (Continuum Project # 17/14979) within the NRL facility.

The high energy pump laser (Continuum Project # 17/14979), shown in Figures 1 & 2 is described in detail elsewhere [28]. Briefly, the laser is initiated with a narrow linewidth fiber laser based on a truly single mode (NKT Photonics, Koheras Adjustik) with an operational power of 85 mW at 1053.390 nm. The narrow linewidth fiber laser is then sent to a programmable optical pulse shaper (Kentech Instruments modulator 10 ns) to create the desired temporal characteristics in the injector laser beam. The initial seed pulse is selected by polarization control for injection into an initial ring cavity. The ring cavity has a 5 mm amplifier Nd:Glass rod with several pass amplification controlled by Pockel's cell which has two states. One state allows continued transmission of the pulse around the ring and the second state kicks the pulse out of the ring with a polarizer. This particular Pockel's cell has been the most problematic for the laser due to the long time on with high voltage creates heat and stress. NRL bought a new component under advisement from Continuum because other similar designs were challenged with this design. The length of time in the cavity was adjusted for stable gain measured with a fast photodiode examination through the leakage of a ring cavity mirror (NRL designed and operated). The stable ejected pulse is amplified by another 5 mm amplifier before expansion to a 19 mm Nd:Glass rod amplifier. Note the second harmonic generation output is ~1 J if operating the pair of 5 mm Nd:Glass rods and the 19 mm Nd:Glass rod only. In order to get to the desired 10 J performance are larger 45 mm rod is required. Prior to the beam getting to the 45 mm laser amplifier Nd:Glass rod protection from gain going back up the laser system is required. In this case, the

output of the 19 mm Nd:Glass rod amplifier passes through a Faraday Rotator for protection prior to the laser beam expansion to 45 mm diameter. The final amplifier is a 45 mm amplifier Nd:Glass rod and a second harmonic generator with dichroic mirrors follow to produce a clean green output. The specifications and delivered performance are shown in Table 1.

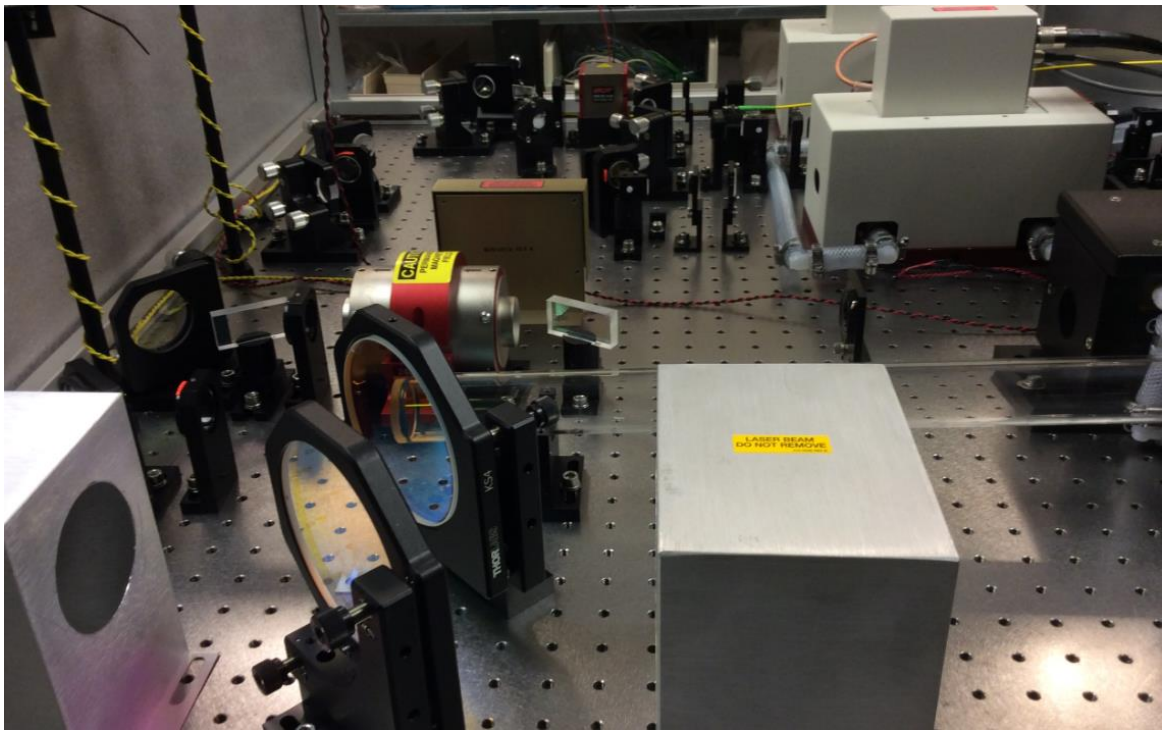

Figure 2. Interior view of Figure 1. the Continuum Project # 17/14979 Laser (10 J Green Nd:Glass Laser). Pictured in the foreground is a second harmonic generation mount (box with Laser Beam Do Not Remove sticker) followed by dichroic high reflectors after output of the 45 mm amplifier. Up from the dichroic mirror pair is the Faraday Rotator after the 19 mm amplifier (black box with hole to right). Farther up in the picture is part of the ring cavity and the two 5 mm amplifier modules. The 5 mm amplifier module closest to view is the one utilized in the ring amplifier. Between the two 5 mm amplifier modules a fiber, which housed the fiber injected laser beam can be seen.

Table 1. Specifications and Delivered Performance of Continuum Project # 17/14979 Laser

	Specifications	Performance
Wavelength	527nm	527nm
Repetition rate	Shot/20min	Shot/20min
Energy	10 J	>10 J
Pulsewidth	3ns	1-6ns
Shot to Shot stability	5% RMS	2.6% RMS
Beam Diameter	< 50mm	~40 mm
Spatial profile	Flat top	Flat top
Divergence	0.5 mrad	<0.5 mrad
Long Term Drift	<5% (RMS) Over 8 hour	2.7% rms over 8 hours
Timing jitter	<100ps RMS	30ps RMS
Pointing Stability	<100 micro rads	88 micro rads
Temporal Profile	Flat top	Flat top
Rise/Fall Time	400/600ps	400/600ps

Initially, the Continuum Project # 17/14979 Laser had two possible applications, one the aforementioned SRRS project as well as Thomson scattering for the Nike facility. The rational for the specific requirements for the purchased laser were as follows. The SRRS experiments require a minimum of 10 J at 527 nm with linear polarization with a pulse width of 3 ns. Adjustability of the laser pulse width to vary the intensity and to evaluate surrogate pulse laser shapes for laser inertial confinement fusion was also desired. The 10 J pulse energy is required to be within a 4 nanoseconds long, this includes the rise time and fall time of the laser temporal profile (500 ps rise time + 3 ns pulse width + 500 ps fall time = 4 ns) and over a beam diameter of less than 5 cm to provide the required intensity for SRRS in air. We prefer a shorter rise and fall time and the ability to maintain constant laser energy with a shorter pulse width. The temporal profile should be square in nature to provide a constant intensity during the main part of the laser pulse to allow both SRRS gain evaluation and for the Thomson scattering application. The pulse length needs to be adjustable for higher intensity required as a diagnostic tool on the Nike laser system due to the need to be converted to shorter wavelength utilizing additional harmonic generation. The temporal jitter needs to be less than 100 ps in order for the proposed laser to be accurately timed to the Nike laser system. A controlled linear polarization is needed to evaluate the polarization dependence of the SRRS process. A single longitudal mode is required with a laser beam divergence of less than 0.5 mrad (preferable to be <0.12 mrad) with a flat-top profile to be representative to an inertial confinement fusion (ICF) laser. The pointing stability is required to be less than 50 microrads in order to accurate place the focal distribution in experiments. The shot to shot stability, or ability for the laser to produce the same pulse energy is less than 5%, so one laser experimental shot and can be easily comparable to another without significant number of shots. The required duty cycle is a shot every 20 minutes for thermal equilibration and the capability of acquiring a reasonable number of data shots daily as well as not extending the time between shots on the Nike laser facility when used for Thomson scattering applications. The delivered performance by Continuum exceeded the parameter requirements put forth by NRL as requirements for the green SRRS experiments and Thomson scattering for the Nike facility.

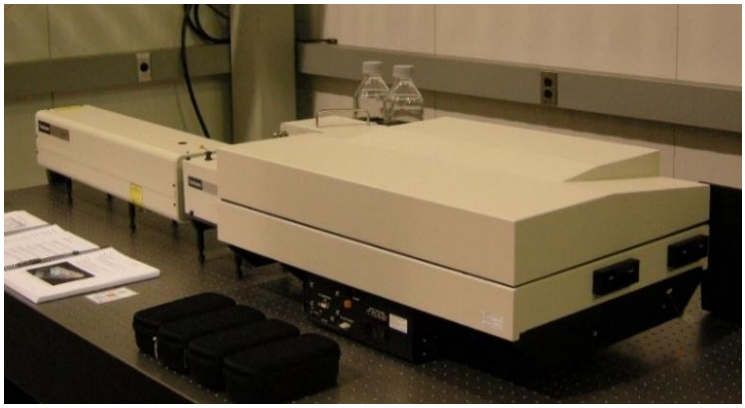

Figure 3. The Continuum Nd:YAG Surelite laser at 355 nm and Continuum Vista laser utilizing Coumarin 500 laser dye employed within the Naval Research Laboratory.

The other critical laser for the SRRS measurements is a pumped dye laser for narrow linewidth tuning with extreme wavelength accuracy and precision. In order to generate the dye laser an externally triggered adjustable repletion rate Surelite Nd:Yag (Continuum) with a pair of harmonic crystals, the first to generate 532 nm and the second crystal to use the generated 532 nm with the fundamental 1064 nm to generate 355 nm. The 532 nm and 1064 nm light is separated with dichroic mirrors. The 355 output is used to pump a Conitnuum Vista for wavelength flexibility shown in Figure 3 and Figure 4 a, b, & c. For the tuning range desired for the green SRRS experiments, precise tuning around 527 nm, the laser dye used was Coumarin 500 (C500). The C500 dye exhibits peak energy at 510 nm with a usable wavelength range from 480 nm to 540 nm. The dye laser has a control personal computer (Figure 4 d.) which controls the linear actuator

grating angle with sub-picometer wavelength precision. The dye laser with Coumarin 500 allowed stable output over the range of rotational Raman lines available for nitrogen and oxygen with the pump laser (Continuum Project # 17/14979) at 527 nm. The dye laser has been shown to be very stable over long durations with steady and reliable output with little maintenance required.

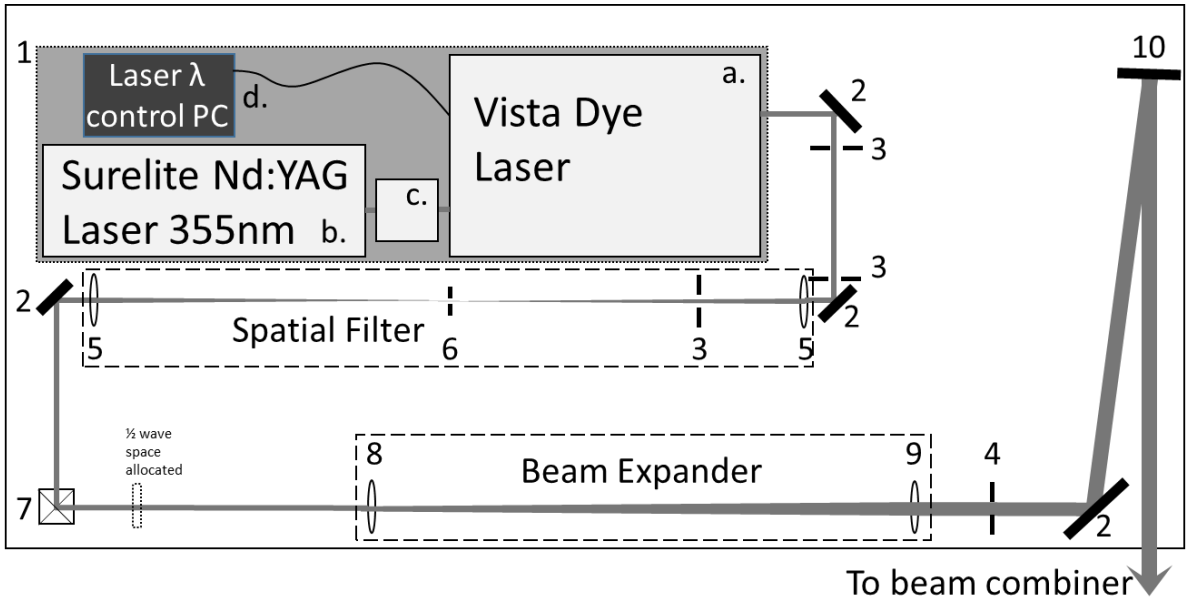

Figure 4. Continuum Dye laser system (1). Computer controlled variable wavelength (d). Surelite (Continuum) Nd:YAG laser with output at the third harmonic, 355nm, supplies energy (b) with dichroic mirrors to separate green and fundamental (c) for Vista Dye laser operated in the green with Coumarin 500 (a). Multiple 45° mirrors (2) and apertures (3) were utilized before a spatial filter with a 450 micron aperture (6) in conjunction of 1 meter focal length lenses (5). A periscope (7) for beam height adjustment and polarization rotation to enter a beam expander composed of a 75 mm focal length lens (8) and a meter length lens (9) eventually followed by variable aperture (4) and 0° mirror (10) to allow precise control on the beam combiner.

2.2 Optical Layout

Over the course of experimental work on the green SRRS experiments many alternate optical configurations were utilized. In this section we will provide a subset of configurations as examples as well as nomenclature to elucidate the experimental work in the results section. All configurations were an attempt to maximize the intensity length product of the pump laser with an overlap of a seed in some cases using both collinear and focal geometries. The dye laser utilized a spatial filter [29] and beam expander for some seeded experiments as shown in Figure 4. The pump laser and seed laser overlap with opposing circular polarization, which is expected to have the highest SRRS gain is shown in Figure 5. Figure 5 shows overlap of beam combining using a cube with two orthogonal polarizations which minimizes the loss mechanism found for laser beam combining. The pump laser utilizes the ‘s-polarized’, the electric field is normal to the plane of incidence, in reflection to maximize the high intensity pump laser. The dye laser transmits with ‘p-polarized’, the electric field is along the plane of incidence, light through the beam combining cube which has greater loss than ‘s-polarized reflection but allows the laser beams to combine. The dye laser seed being slightly diminished has less experimental impact than diminishing the high intensity pump laser. To initiate circular polarization a quarter waveplate was utilized, with the circular polarization rotation in opposing directions originating from the original orientation. The circularly polarized light or linear polarized light is propagated to the other end of the room to allow sufficient gain of SRRS in self-seeded or seeded configurations. To increase the signal size of SRRS if the pump laser intensity is insufficient or to allow the seed laser to be at higher fraction of the pump laser additional path length opportunities were created.

Figure 6 shows a focal geometry using a pair of eight meter focal length lenses passing back and forth across the room prior to reaching the induced SRRS diagnostic table. The first eight meter focal length lens focuses the laser beam and the second eight meter focal length lens allows re-collimation of the laser beam. In order to make spectral measurements of the high intensity laser beam attenuation of the laser beam was conducted with a 4% pick-off optic followed by neutral density filters amongst other available attenuation methods to avoid 'ghost pick-up' and maximize the CCD response of the Hyperfine spectrometer. In addition, the optical layout in Figure 6 can be utilized with linear polarization by removing the last quarter wave plate prior to propagating towards the induced SRRS diagnostic table.

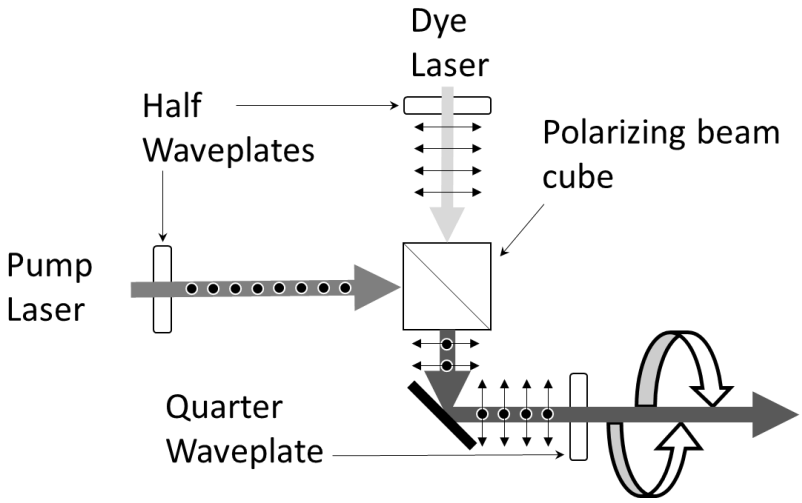

Fig 5. Seeded beam is formed by combining the S polarized (●) Pump (Continuum Project # 17/14979 Laser) laser reflecting through and the P polarized (↕) variable wavelength dye laser transmitting through a polarizing beam cube. The resulting combined and cross polarized beam transmits though a quarter wave plate resulting in a predominantly circularly and oppositely rotating polarized beam.

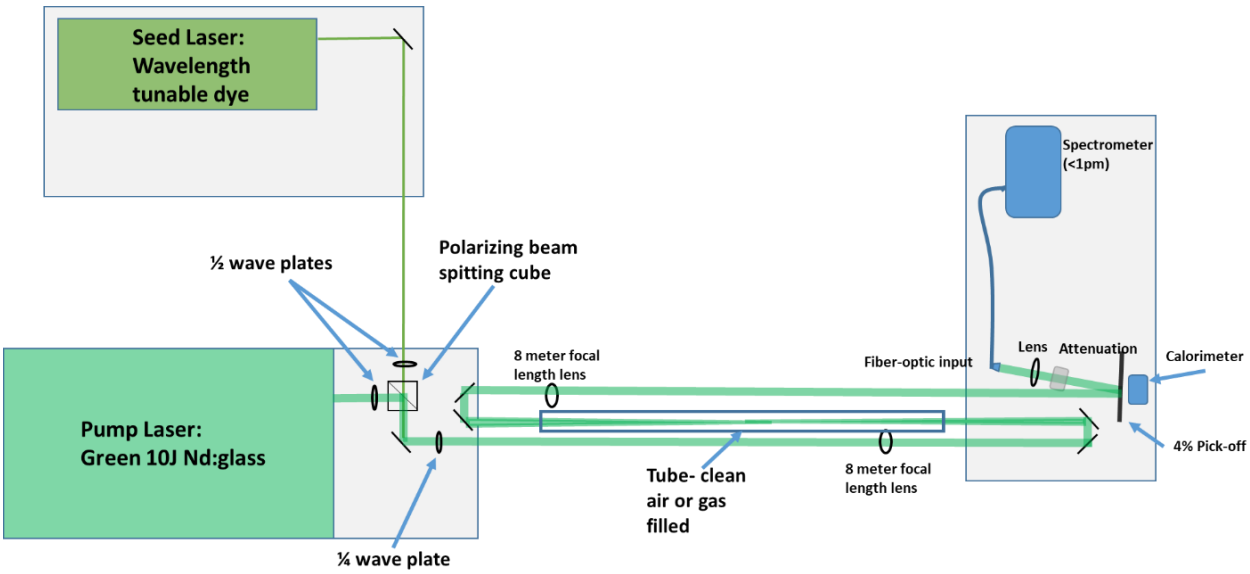

Figure 6. Diagram of SRRS experimental setup used for focal geometry in both seeded and self-seeded cases utilizing linear, orthogonal, and circular polarization for seeded and self-seeded SRRS. Propagated beam passes though focus in controlled clean air tube. Diagnostic measurment geometry for induced SRRS are shown on optical table on right of figure.

2.3 Diagnostics

The green SRRS experimental laboratory has several diagnostics for measurement including spectral frequency, intensity, energy, spatial imagining and temporal-spectral response. The spectral diagnostics include two spectrometers, a high resolution spectrometer, Hyperfine Spectrometer, from Light Machinery and slightly lower resolution over a larger wavelength span spectrometer, StellarNet, from StellarNet Inc. The Hyperfine Spectrometer has less than 1 picometer resolution, 5 points per picometer steps, over a 10 nm wavelength band adjustable from 500 nm to 600 nm. For a calibration a broadband white light source is required. We used a Dolan Jenner Industries Fiber-Lite High Intensity Illuminator Series 180 for the broadband white light source, which worked very well. In addition, for calibration a narrow bandwidth laser is required we used a 532.0 nm continuous wave Coherent DPSS 532 Laser. The custom software for the Hyperfine Spectrometer read the raw image and converted to laser wavelength and intensity. For a larger range evaluation of the SRRS generated lines a StellarNet HR-NIR4-7 spectrometer was used utilized. The specifics for the StellarNet spectrometer include 2400 g/mm grating, and 7 nm slit which allowed a range of 100 nm with 2051 points with a resolution less than 0.05 nm. Timing overlap and pulse shape was measured with silicon photodiodes (Thorlabs DET 10A). Calorimeters were used to measure the laser energy. Spatial imaging measurements of the laser beam for evaluation of the shot to shot reproducibility of the beam spot were made with a gated camera (LA Vision camera [30]). A time resolved streak camera was also available for this project (Hofstra Group).

3. MEASUREMENTS

Many measurements have been conducted for green SRRS evaluation. In this section we will concentrate on the most significant findings to generate substantial bandwidth and characteristics of the generated bandwidth dependent on experimental parameters. Substantial more data was taken at the 0.5-1.0 Joule energy without operating the final 45 mm Nd:Glass rod of the pump laser. The full energy 10 Joule output using the 45 mm Nd:Glass rod had a shot rate of every 20 minutes and lower certainty on the shot to shot reproducibility. Due to operating at lower energy, thus lower intensity, the focal geometry configuration showed substantial more SRRS signal and was utilized more often.

3.1 Broad Bandwidth Generation

The ability to generate substantial bandwidth, measured with two different spectrometers, with the NRL laser and configuration is shown in Figure 7. The bandwidth has a range of 17 THz using components of anti-Stokes rotational lines, the pump laser and significant stokes rotational line generation. The anti-Stokes rotational line radiation is the wavelength range shorter than the pump wavelength of 526.4 nanometers. The significant Stokes rotational line radiation is the intensity extending at longer wavelengths than the pump laser wavelength. The laser configuration for the data was utilizing all the amplifiers of the Continuum #14979 laser, including the 45 mm Nd:Glass rod amplifier to obtain close to 10 Joules. No seed or dye laser was utilized to generate the very large bandwidth. A quarter wave plate was utilized to generate circularly polarized light. An eight meter focal length lens was used to focus the laser beam, which has a spot size large enough to avoid ionization breakdown. The pulse length was 3 nanoseconds. The light was collimated and captured into a fiber coupler for the spectrometers. The two spectrometers used to measure the generated SRRS light co-propagating with the pump laser beam was a Hyprefine spectrometer and StellarNet spectrometer. As shown in Figure 7 the StellarNet spectrometer captures the entire bandwidth of light within the observation range of the spectrometer. The shaded part of Figure 7 shows a region where the data was beyond the ten nanometer window utilized for the Hyperfine spectrometer range. The StellarNet spectral resolution utilized does not allow the individual rotational lines to be determined. Whereas the Hyperfine spectrometer can determine individual rotational Raman transition lines. The areas of increased line density and line intensity measured by the Hyperfine spectrometer correlates well with the StellarNet spectrometer observable response by binning the line density and line intensity as appropriate.

In the range outside of the Hyperfine spectrometer measured by the StellarNet spectrometer there is a significant amount of intensity extending over several nanometers.

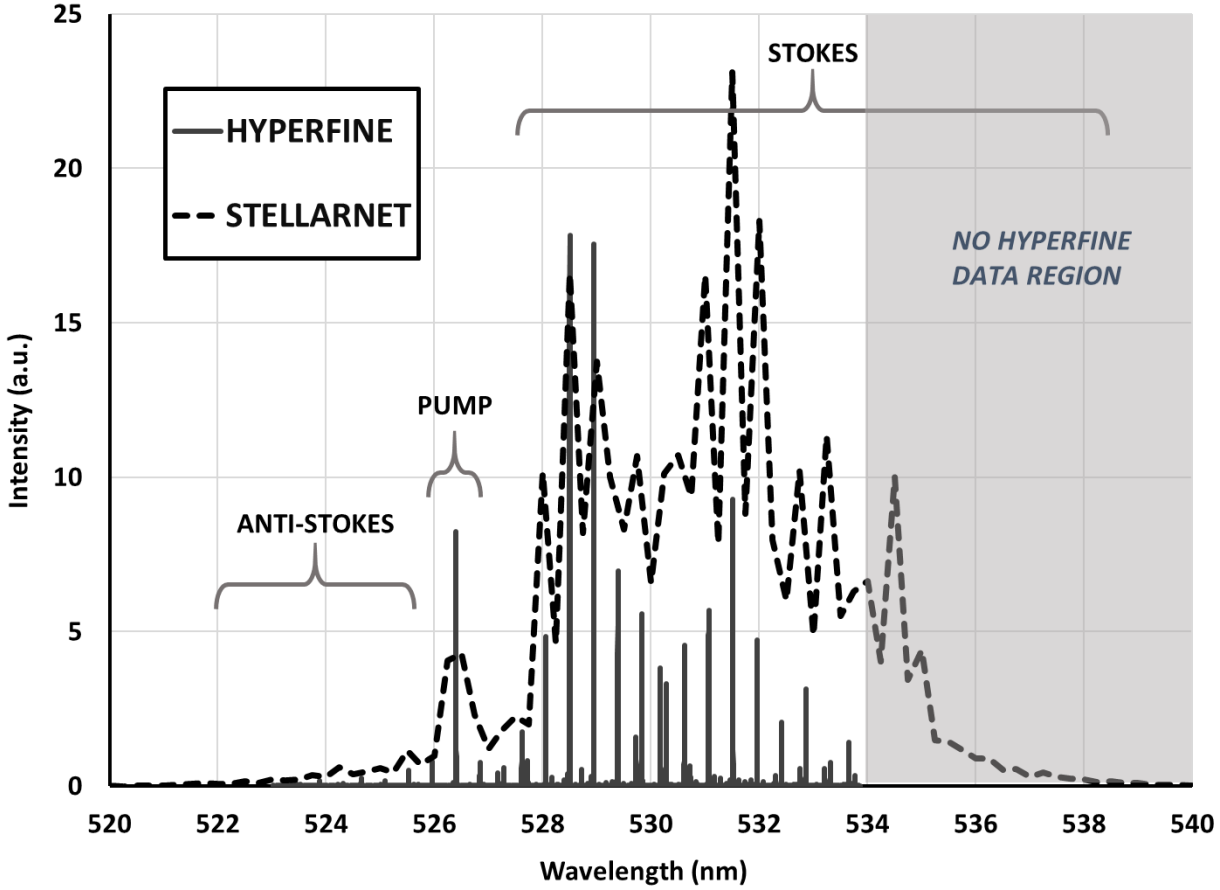

Figure 7. SRRS generated bandwidth of self-seeded circularly polarized though focus using the maximum energy of the pump laser with the 45 mm Nd:Glass rod. Stellarnet spectrometer (dotted line) shows a range of 17 THZ generated bandwidth that extends past the 10 nm measurement range of the Hyperfine spectrometer (solid line). The wavelength region outside of the Hyperfine data region at 534 nm is shaded in grey. The pump laser was at wavelength near 526.4 nm from the measurements using the spectrometers. The rotational Raman lines at shorter wavelength than the pump are anti-Stokes, whereas the longer wavelengths relative to the pump wavelength are the Stokes rotational Raman lines.

A more detailed and expanded view of the Hyperfine measured spectrum is shown in Figure 8. Using a rotational constant (B) for nitrogen of 1.979 cm^{-1} is instructive in line identification in Figure 8. The rotational constant used for nitrogen is less than the expected value of 1.98950 cm^{-1} [31], but accuracy of the Hyperfine spectrometer linearity over the region of the nitrogen rotational Raman lines has not been confirmed, which could account for the discrepancy. The single rotational Raman transition are denoted with an X position relative to the pump using the rotational constant (B) as 1.979 cm^{-1}. The labeling of the transition such as j=8 represents the J 8→10 transition. The shift in frequency for Stokes rotational lines is 2B(2j+3) in wavenumbers (cm^{-1}). Note the shift in frequency for anti-Stokes which was omitted from the Figure 8 for clarity is 2B(2j-1). The X positions have a noticeable signature in the observed spectrum of all even transitions as expected from j=4 up to j=24. The j=8 and j=10 transitions are among the strongest measured transitions as expected. In addition we can also see the second Stokes lines marked with O in Figure 8. These transitions occur at frequencies 2*(2B(2j+3)) where for example j=6, j=6 is twice the shift of a single j=6 transition. Also the frequencies for the odd j's of second Stokes in the formula of the previous sentence are also observed due to the combination of a single transition and another single transition of a different transition combining as in the j=6, j=8 combination or equivalent j=8, j=6 combination. Also the frequency of a single second Stokes as in j=10, j=10 is equivalent in frequency shift as j=8, j=12 or j=6,

j=14 and so on. Therefore the labeling the labeling in Figure 8 is representative of a possible line due to multiple rotational Raman Stokes lines from nitrogen. In Figure 7 the StellarNet spectrometer showed light outside of the available rang using the Hyperfine spectrometer most likely indicating third Stokes lines and possibly fourth Stokes lines or higher were generated using the focal geometry method. We did observe the 8B intercombination line as previously observed by Averbakh [32] and Dixit [33].

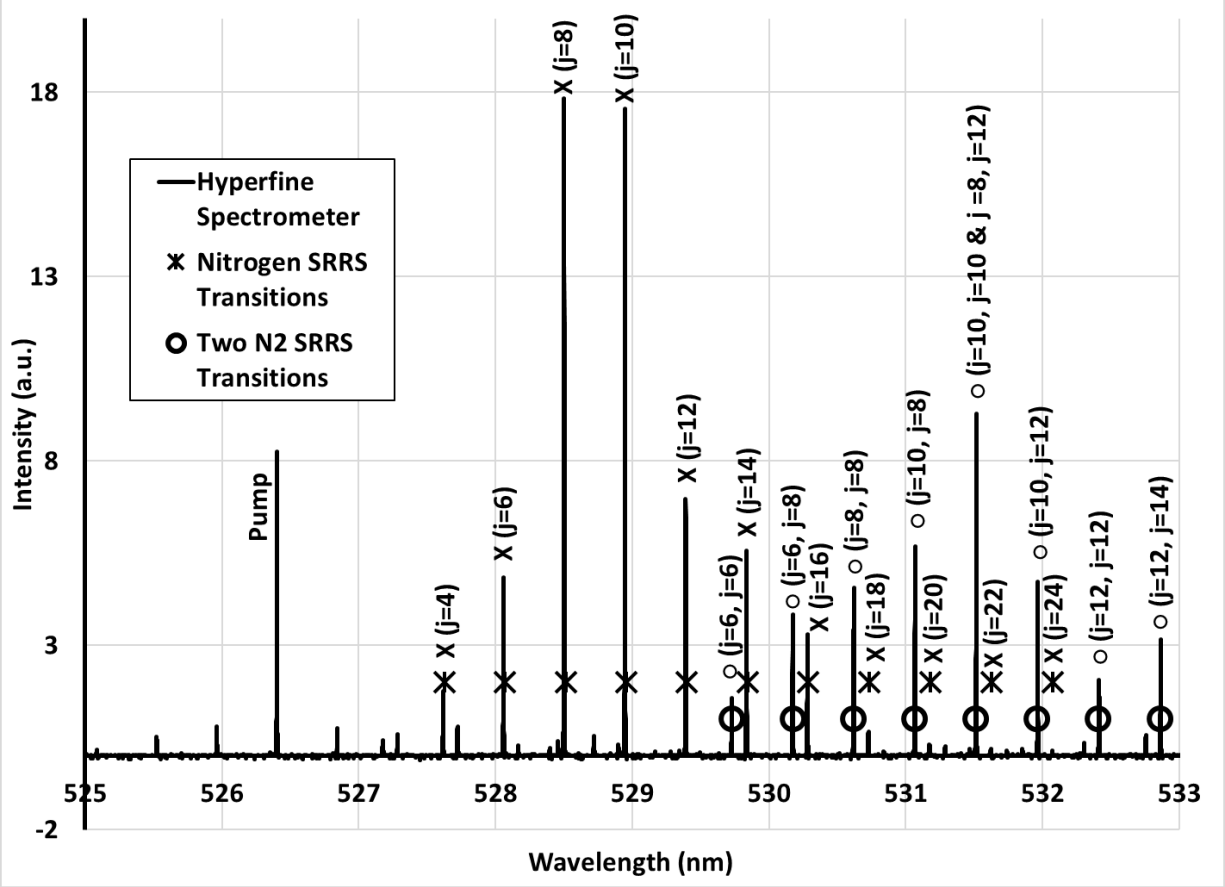

Figure 8. Expanded view and labeling of key transitions form the Hyperfine spectrum shown in Figure 7. Estimate of the rotational constant (B) for nitrogen in these measurements is 1.979 cm^{-1}. The X symbol are the observed lines from a single nitrogen rotational Raman transition labeling (j=8) as the J=8→10 transition. The O symbol represents line generated by 2 or more combination of lines, note the frequency of (j=10, j=10) is the same as (j=8, j=12) or (j=12, j=8) and so on. We did not specify all the possibilities for each multi-photon line.

3.2 Seeded Anti-Stokes

The dye laser was tuned to the exact frequencies measured for the self-seeded rotational Raman lines of nitrogen to examine amplification in a laser seeded SRRS configuration. Experiments were conducted utilizing a focal geometry, eight meter focal length lens, with less than 1 Joule of laser energy due to operation without the 45 mm Nd:Glass amplifier rod. The seed laser beam and the pump laser beam were circularly polarized one beam clockwise polarization rotation and the other laser beam counter clockwise polarization rotation, which will define here as counter-circular-polarization-rotation. Both Stokes and anti-Stokes seeding by the dye laser were investigated. In Figure 9, the integrated counts is a summation of all the response for a given line width and plotted on a log scale relative to wavelength. The pump laser wavelength is at 526.4 nm. The Stokes seed provide significant more gain as opposed to ant-Stokes seeding. Even though the seed was provided at anti-Stokes rotational lines no light was observed at the initial

wavelength. The anti-Stokes light was completely converted to Stokes light at the same rotational transition seed. In one case for the Stokes seed at j=8 a small amount of anti-Stokes light was generated. The seeded case at j=6 was higher than j=10, which was significantly different than the self-seeded case with higher laser energy shown in Figure 8. The linewidths of the seed laser pump laser and the rotational Raman transitions in this configuration were measured and shown in Figure 10. The transitions follow the narrower seed laser as expected due to the expected rotational Raman transition is narrower than the pump laser linewidth.

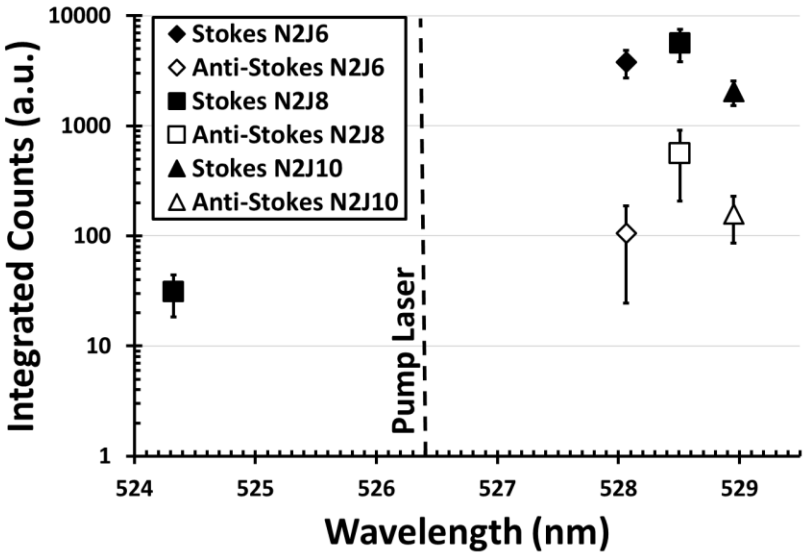

Fig. 9. Observed seeded SRRS growth with variable dye seed laser wavelength set to N_2 rotational Ramen Stokes lines J=10(▲), J=8(■), and J=6(◆) and anti-Stokes lines J=10 (△), J=8 (□), J=6 (◇) with respect to pump laser. The integrated counts is a summation of all the response for a given line width and plotted on a log scale relative to wavelength.

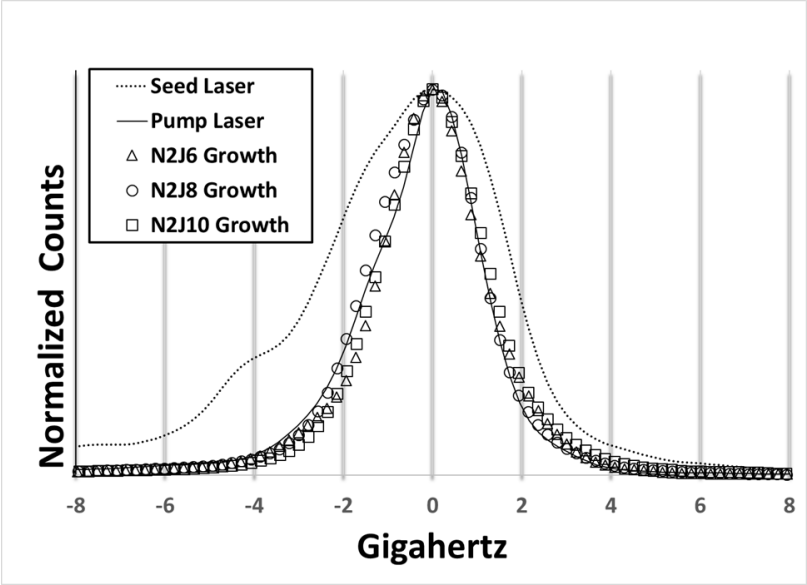

Figure 10. The measured linewidth with the Hyperfine spectrometer for seeded SRRS with counter-circular-polarization-rotation between the pump laser beam and the seed laser beam. The measured transition linewidth is the same as the narrower laser beam provided due to the rotational Raman transition being extremely narrow.

3.3 Self-Seeded Circular vs. Linear Polarization

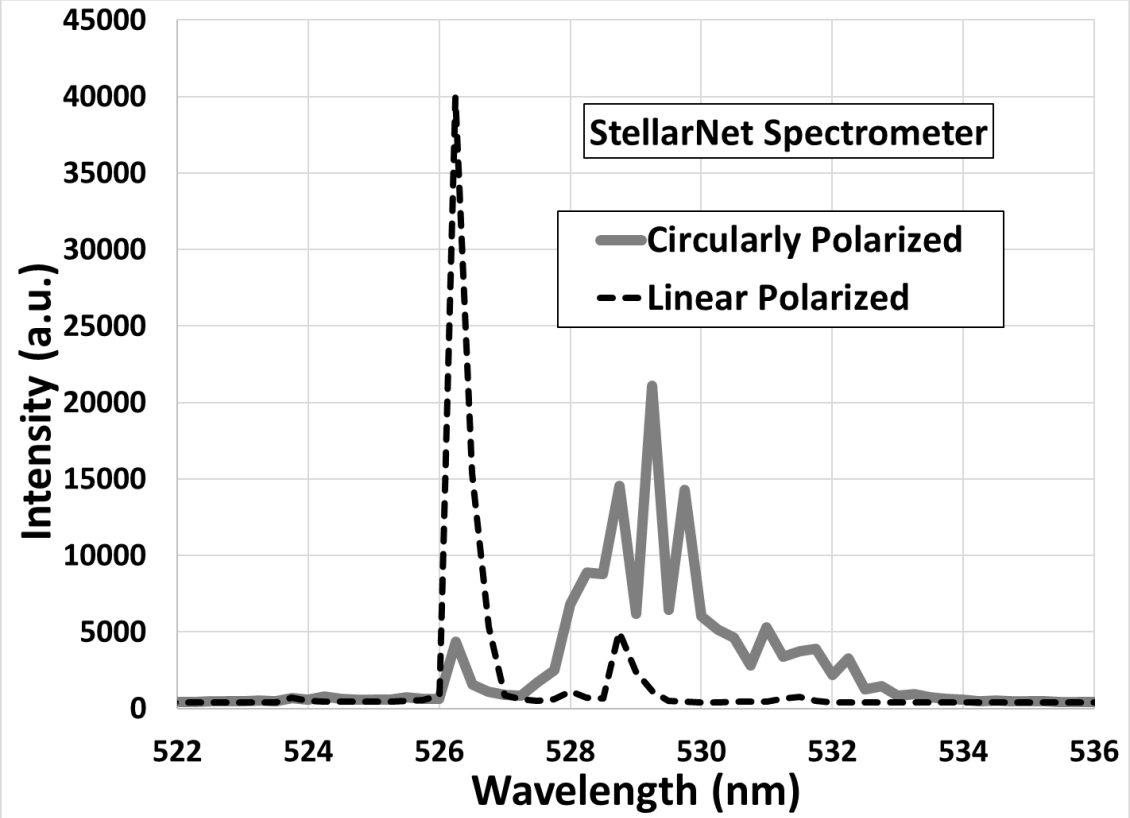

Figure 11. SRRS response for circularly polarized light shows substantial conversion of the pump laser beam measured with the StellarNet spectrometer. Whereas in the case of linear polarized light the SRRS generation is limited and the laser energy remains in the pump beam.

Expectation of greater SRRS gain utilizing circularly polarized light compared to linearly polarized light has been documented previously [3,20]. Recently a theoretical description of stimulated rotational Raman scattering of arbitrarily polarized broadband light has been reported [3]. Higher gain of SRRS has many advantages for applications, such as using on an inertial confinement laser fusion facility, reducing the intensity or path length required generate a SRRS broad bandwidth spectrum. In addition higher gain will also shorten the required path length in maintaining SRRS development in the transient regime where the spatial disruption of the laser beam will be significantly reduced or nearly imperceptible. To examine the effect of polarization a straightforward experiment with circularly polarized light utilizing the entire output of the Continuum #14979 laser, including the 45 mm Nd:Glass rod amplifier with a 8 meter focal length lens as described in broadband generation followed with an experiment without the quarter wave-plate for linearly polarized light using the same 8 meter focal length lens focal arrangement to generate self-seeded SRRS. Both spectrometers, StellarNet (Figure 11) and Hyperfine (Figure 12) showed substantial SRRS generation for the circularly polarized light case and very limited SRRS generation for the linear polarized case. In the linear polarized case the energy remains at the pump wavelength with a very modest amount of transition to j=10 single nitrogen rotational Raman line. We have been unable to make a determination of why the observation of only this generated frequency in the linear polarized self-seeded case. For the case of circularly polarized light the breadth of the SRRS generated light has higher intensity and over many more frequencies. There is evidence of light out to 533 nm, which requires multiple SRRS transitions in order to reach as examined in the Broad Bandwidth Generation section discussed above. The significant difference is related to two phenomena, exceeding threshold and gain. The threshold is generating the first

self-seeded photon at a nitrogen rotational Raman transition. The gain is after the initial frequency has been generated the increase in the number of photons due to having a seed to stimulate the frequency to generate more photons at the same frequency. Circularly polarized light is advantageous for creating a lower intensity length product to initiate nitrogen rotational Raman transitions and the required intensity length product to generate gain.

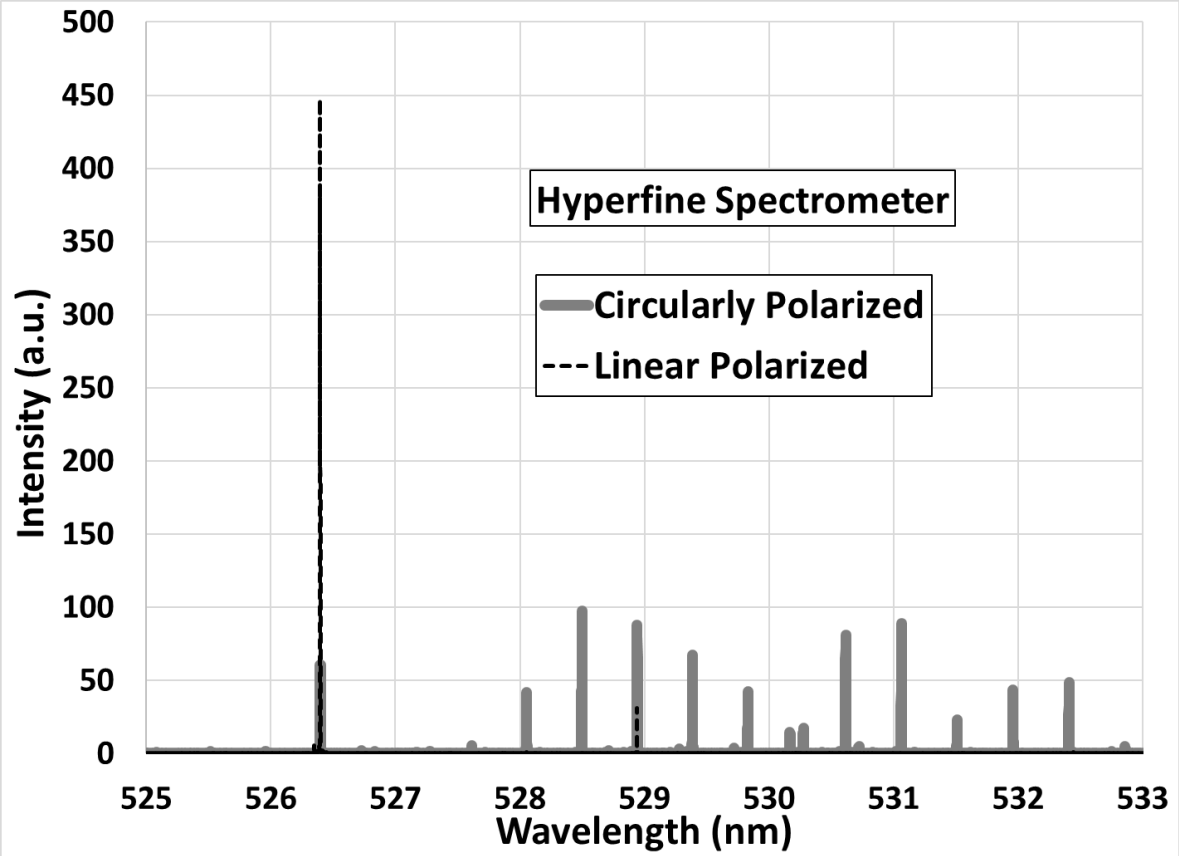

Figure 12. The Hyperfine measured response of circularly polarized light creates many single nitrogen rotational Raman lines as well as lines generated by combining the initial generated SRRS photons. Whereas the linear polarized example shows most of the light remain in the pump laser frequency with some light generated in the Stokes j=10 transition.

4. MODELING CONSIDERATIONS

Substantial efforts for modeling SRRS accurately has been previously reported [2,3]. Examining the SRRS with a narrowband green laser light in a focal geometry required some changes. The focal geometry requires a Talanov Lens transformation [34] and significant implications on Stokes-Anti-Stokes coupling, which will be briefly discussed in the next subsection. In addition, the laser light described in the measurements are much coherent than beam smoothing technique of induced spatial incoherence (ISI) envisioned to use with excimer lasers. We modified an earlier version of NRL's SRRS code for utilization of one beam on the University of Rochester Omega Laser facility.

4.1 Talanov Lens Transformation

In order to simulate diverging or converging laser beams significant amount of memory is required unless a transformation is conducted [35]. A Talanov Lens transformation [34] removes rapid spherical phase

curvature and allowing simulation of laser beams as if laser beams are collimated [35]. Examination of a generalized treatment similar to Sziklas & Siegman [36], Suydam [37] and Marburger [38] suggests that spherical beam convergence does not suppress Stokes-Anti-Stokes coupling. However Stokes-Anti-Stokes coupling can be suppressed going through a focal geometry as the data in the Measurement section in this Memorandum as well as the work by Eimerl [1]. Collimated laser beam experiments [39-41] show parametric suppression due to Stokes-Anit-Stokes coupling. The evaluation of the Eimerl work [1] as well the present focal geometry experiments need a Talanov Lens transformation [34] or something similar in order to evaluate with present day available computing [35].

4.2 LLE Omega Example

NRL's stimulated rotational Raman scattering (SRRS) code was further developed to investigate implementation of using SRRS on the University of Rochester LLE Omega facility at LLE. This investigation has included modification of the code with wavelength changes from 248 nm to 351 nm, and 527 nm. In order to change the wavelength in NRL's SRRS code we determined important optical constants for the gas media of the SRRS propagation (air) for each wavelength for group velocity dispersion, steady state nonlinear index of refraction (n_2), instantaneous nonlinear index of refraction (n_2) and Rayleigh Power Attenuation shown in Table 2. We conducted studies varying initial bandwidth of both seed laser and pump laser, angle between the seed laser and pump laser, and varying the frequency of the seed (wavelength). The initial evaluation showed a minimum 1 Joule seed with compressing the University of Rochester LLE Omega laser beam diameter from 28 cm to 20 cm at lower frequency shift of 2.280 THz (corresponding to j=8 for nitrogen) from the center frequency of the University of Rochester LLE Omega laser system provided the best results over an 18 meter path length. Modifying the University of Rochester LLE Omega laser system with a quarter wave-plate and providing a circularly polarized light with an oppositely circularly polarized seed laser provides the greatest conversion to the desired SRRS frequencies. In addition, we acquired and tested Ver 5.9 GLAD software from Applied Optics Research for comparative testing for SRRS performance to the NRL code. In conclusion calculations show significant conversion from the pump frequency to SRRS bands at -6.84 THz, -4.56 THz, -2.28 THz, 2.28 THz, 4.56 THz and 6.84 THz (-6.84 THz and 6.84 THz were significantly lower in intensity) with the bandwidth of the individual bands directly dependent on the laser bandwidth of the University of Rochester LLE Omega laser facility entering the 18 meter propagation. The LPSE-CBET simulations indicate that significant suppression of CBET on University of Rochester LLE Omega will occur with bandwidths above 2 THz, which appears to be well within the bandwidths attainable with this approach. A sample simulation of the spectrum of a University of Rochester LLE Omega beam with SRRS-enhanced bandwidth is provided in Figure 13.

Table 2. Important Optical Constants for Air Used

Laser	1w	2w	3w	KrF
Wavelength (nm)	1052.6	526.3	350.95	248
WL_L (cm)	1.0526×10^{-4}	5.263×10^{-5}	3.5095×10^{-5}	2.48360×10^{-5}
GVD (ps^2/mm)	1.4486×10^{-7} [42]	3.4146×10^{-7} [42]	6.1×10^{-7} [42]	1.2×10^{-6} [42]
Steady state n_2 (cm^2/GW)	4.2×10^{-10} [43]	3.01×10^{-10} [44] (800 nm)	5.36×10^{-10} [44] (400 nm)	$9.2166525 \times 10^{-10}$
Instantaneous n_2 (cm^2/GW)	7.9×10^{-11} [45] (1250 nm)	7.9×10^{-11} [45] (800 nm)	9.3×10^{-11} [45] (400 nm)	2.6×10^{-10}
Rayleigh Power Attenuation /cm [46]	2.1×10^{-6}	3×10^{-6}	4×10^{-6}	7.5×10^{-6}

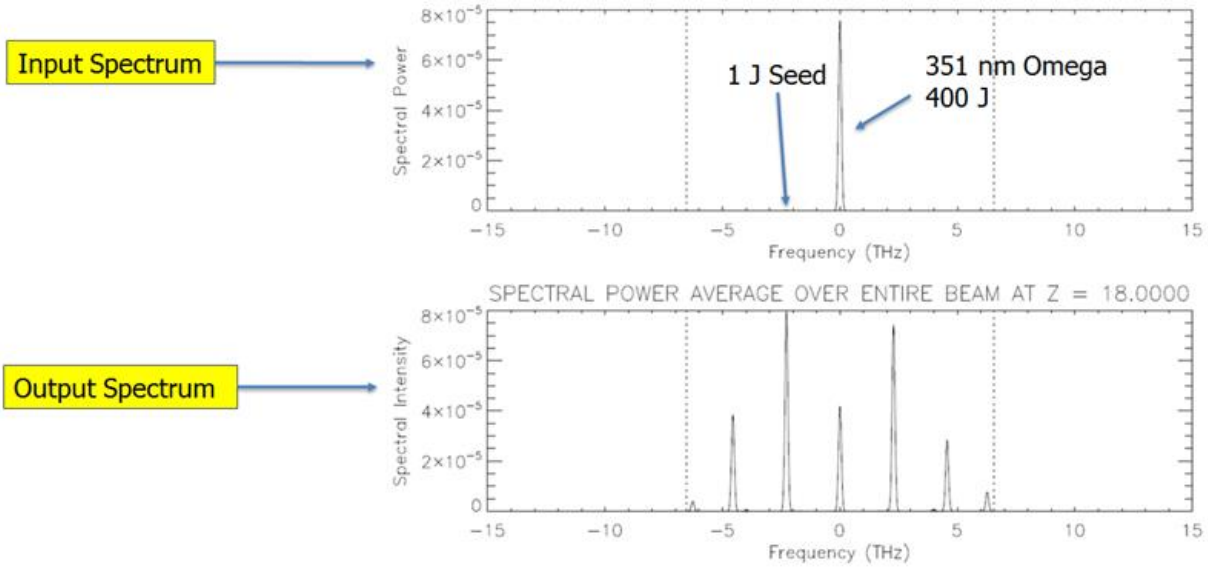

Figure 13: Simulation of the SRRS induced bandwidth of one University of Rochester LLE Omega beam seeded by a 1 J laser beam with an appropriately shifted wavelength. The University of Rochester LLE Omega beam was reduced in diameter (factor of two in area) and circularly polarized (e.g. by a quarter wave plate) to increase the SRRS gain.

5. DISCUSSION

5.1 Measurements and Modeling Discrepancies

The SRRS measurements conducted here were in the focal geometry. Attempts of generating SRRS with a seed or a self-seeded in a collimated laser beam geometry were unsuccessful. The interpretation after examination of the intensity length product implies another factor contributes to the cause. The Stokes-Anti-Stokes coupling suppression in the focal geometry as described in the Talanov Lens Transformation section is instructive on a possible cause. The NRL model used in the section entitled, LLE Omega Example, was prior to and did not contain the Stokes-Anti-Stokes coupling as in Lehmberg [3]. Parametric suppression can be significant in a collimated geometry which limits the generation of Stokes rotational Raman lines. Another consideration is beyond the Stokes-Anti-Stokes coupling is the generated Stokes radiation vector (k-vector) not being exactly collinear with the pump laser beam. We were hoping the seed would help guide the gain in directionality, but if self-seeded generated light has higher intensity off-axis than the seed laser along the travel of the collimated laser beam the Stokes radiation would not reach the diagnostics. The process could have off-axis cones where the light moves outside the laser beam and in the experimental measurements would be an additional scattered light component. A dispersion material can be added to assist the Anti-Stokes k-vector to overlap with a pump laser beam to convert 20% of the pump light to Anti-Stokes [47]. The off-axis cones or simply not having the Anti-Stokes k-vector stay overlap with the directionality of the pump laser beam could account for the lack of Anti-Stokes light in our experiments as well.

Measurements with low intensity sources exhibit clear Anti-Stokes and Stokes nitrogen rotational Raman light with only small difference intensity between Stokes and Anti-Stokes radiation. At high laser intensities as exhibited in this work the measured light signal from nitrogen stimulated rotational Raman scattering processes are dominated by the Stokes radiation at longer wavelengths than the initial pump wavelength. Figure 7 shows very small amount of Anti-Stokes light compared to Stokes light. In addition, Figure 9 shows experimental results of seeding at an Anti-Stokes line with all the energy going to the Stokes line directly and no gain in the seeded Anti-Stokes line. The experimental result is significantly different than

Figure 13 modeling of Anti-Stokes seed in Omega laser beam line with reduced diameter where multiple orders of Anti-Stokes and Stokes radiation was predicted to occur with near symmetry around the pump wavelength. Clearly, the Stokes-Anti-Stokes coupling was not accurate in the earlier modeling as exhibited in Figure 13. Even though corrections to the Stokes-Anti-Stokes coupling has occurred in the model, we have not tried to reexamine the experimental data presented here. Thus further investigation is warranted on this topic, especially in finding the appropriate k-vector and dispersion requirements to be co-propagating with the pump laser beam is critical [47]. Again a difference is the collimated propagation in the modeling and the focal geometry used in the experiments may have more differences than originally conceived. Another discrepancy is off resonance seeding outside the available bandwidth of the seed laser still caused a response to nearby rotational Raman levels which will be published at a later date.

5.2 Broad Bandwidth Generation Additional Considerations

The unique diagnostic capability at NRL to have high resolution for the extended stimulated rotational Raman transition lines is unique over multiple orders of lines. Lower resolution measurements of multiple orders has been made previously by others [48]. For line identification, polarization could be used due to the fact the seed laser and the pump laser can have two different polarization states an example using circular polarization in opposing directions, shown in Figure 14. The different polarization states could allow increased confidence in line identification. The process of separating polarization states described is not straightforward for the circular or version of elliptical polarized light, but would be straightforward with linear polarization states. The significant broad bandwidth generated may not be all in the transient regime as intended, where saturation effects could occur. The aspect of saturated transitions that is the most concerning is significant changes to the spatial profile and hot spots where SRRS is generated in copious amounts and generate hot spots [49,50]. We do not adequately investigate the effect of the spatial profile after generation of the broad bandwidth. We were able to propagate the beam a significant distance after the focal geometry and couple to the diagnostics. We did not notice severe laser beam non-uniformity, but we do not measure the laser beam profile before and after SRRS generation to the scale required for adequate evaluation to be used by an ICF/IFE implosion facility.

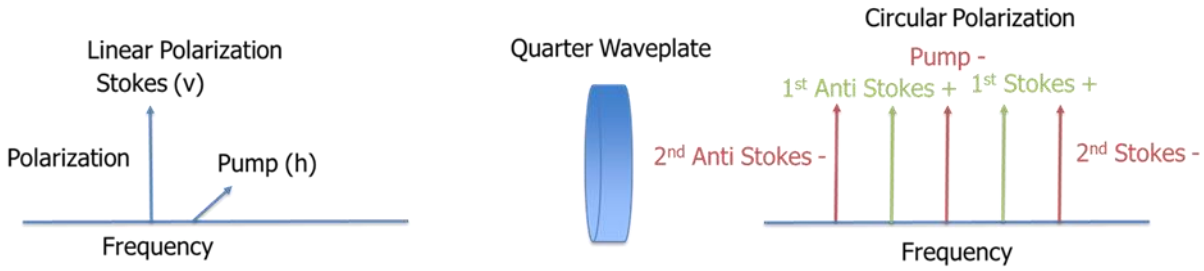

Figure 14. Schematic on opposing circular polarization generation and output. The pump and 2nd order Anti-Stokes and 2nd Order Stokes has the same polarization whereas the 1st order Stokes and 1st order Anti-Stokes have the opposing rotation direction.

5.3 Potential Impacts on Laser Plasma Instabilities

The potential benefit impacts of broader bandwidths for laser plasma instabilities have been described elsewhere [41-53]. Bates et al. [54] examine the effect of using N_2 SRRS in LPSE simulations. The results reported were the SRRS in nitrogen was at least as effective at suppressing cross beam energy transfer (CBET) as 5 THz (Gaussian) laser bandwidth [54]. The broad bandwidth spectrum generated in Figure 7 is considerably larger shift and broader spectrum than used in the LPSE simulations. We would expect only improved performance of mitigating laser plasma instabilities with the larger bandwidth generated spectrum. The nitrogen SRRS method to generate broad bandwidth is not limited to a specific frequency. The effectiveness and ability for SRRS in nitrogen is dependent on the parameters shown in Table 2, which

do change as a function of wavelength. In addition, finding the actual steady state n_2 and instantaneous n_2 at a specific frequency can be a challenge and approximations are used which is less than ideal for accurate modeling of the SRRS generated in a given condition. Therefore improvement on air parameters at various wavelengths would be helpful to distinguish if a nitrogen SRRS broad bandwidth generation is plausible at a given pump laser wavelength for laser plasma instabilities mitigation. A more positive point of view is to find out what materials need to be added to change dispersion to improve overlap and gain to get the desired broad bandwidth needed with sufficient SRRS gain and avoid spatiotemporal challenges. Another possible method of broad bandwidth generation is to use nitrogen SRRS in conjunction with other promising bandwidth generation processes [55].

6. NEXT STEPS

The suggested next steps have been mentioned throughout the document. We will present a brief list of critical next steps for ICF/IFE applications using nitrogen (air) SRRS broad bandwidth generated light. The evaluation of the spatiotemporal dynamics are critical. The present understanding shows there is much subtle complexity which we have not fully examined [50]. The difference between the modeling and the measurements need to be refined to get better agreement. Better measurements of the steady state n_2 and instantaneous n_2 for possible laser implosion wavelengths would be a benefit. Improved understanding of the conditions required for Stokes-Anti-Stokes coupling mitigation would be beneficial. The possibility of fast ignition or other ultrashort pulse fusion efforts leads one to examine the effect of pulse width on nitrogen SRRS broad bandwidth generation. Efficient Raman conversion is possible for ultrashort pulses, which are much shorter than the transverse relaxation time of the medium. Attainment of conversion efficiencies for Raman with ultrashort pulses need new development to be comparable with nanosecond range laser pulses [56].

7. CONCLUSIONS

The U.S. Naval Research Laboratory has developed a method to change the laser spectral width from a very narrow frequency bandwidth ~3 GHZ at full width half maximum to a range of at least 17 THZ in frequency bandwidth utilizing a stimulated rotational Raman scattering process (SRRS). The greater than 3 orders of magnitude (5000 times) in spectral range was achieved utilizing propagation in air and taking advantage of the SRRS response of nitrogen and oxygen. The SRRS process can be enhanced in focal geometry utilizing elliptical (circular) polarization relative to linear polarization. Seeding higher frequency Raman (anti-Stokes) transitions of air diatomic molecules can generate measurable light at equivalent lower frequency Raman (Stokes) transitions. The ability to increase bandwidth for solid state lasers utilizing an inexpensive medium such as air offers potential to be utilized in laser fusion ignition scale facilities to mitigate laser plasma instabilities. Mitigation of laser plasma instabilities (LPI) in a controlled manner with broad bandwidth generation offers the opportunity to increase the parameter space available for successful ICF/IFE implosions.

REFERENCES

1. D. Eimerl, D. Milan, J. Yu, 1993, “Large bandwidth frequency-converted Nd:Glass laser at 527 nm with $\Delta\nu/\nu$=2%,” Physical Review Letters 70(18) 2738-2741. doi: 10.1103/PhysRevLett.70.2738

2. J. Weaver, R. Lehmberg, S. Obenschain, D. Kehne, M. Wolford, 2017, “Spectral and far-field broadening due to stimulated rotational Raman scattering driven by the Nike krypton fluoride laser,” Applied Optics 56(31), 8618-8631. doi: 10.1364/AO.56.008618

3. R.H. Lehmberg, M.F. Wolford, J.L. Weaver, D. Kehne, S.P. Obenschain, D. Eimerl, J.P. Palastro, 2020, "Stimulated rotational Raman scattering of arbitrarily polarized broadband light," Physical Review A 102(6), 063530. doi: 10.1103/PhysRevA.102.063530

4. S.E. Wurzel, S.C. Hsu, 2022, "Progress toward fusion energy breakeven and gain as measured against the Lawson criterion," Physics of Plasmas 29(6), 062103. doi: 10.1063/5.0083990

5. S. Atzeni, J. Meyer-ter-Vehn, *The Physics of Inertial Fusion Beam Plasma Interaction, Hydrodynamics, Hot Dense Matter* (Clarendon. Oxford 2004).

6. A. Zylstra, N. Alexander, R. Bahukutumbi, R. McBride, W. Meier, P. Seidl, M. Wolford, L. Yin, 2022 "IFE Science & Technology Community Strategic Planning Workshop Report," Community Report https://lasers.llnl.gov/nif-workshops/ife-workshop-2022.

7. P. Michel, *Introduction to Laser-Plasma Interactions* (Springer International Publishing. New York 2023).

8. S. Eliezer, *The Interaction of High-Power Lasers with Plasmas* (Institute of Physics Publishing. Bristol 2002).

9. W. Kruer, *The Physics Of Laser Plasma Interactions*, Frontiers in Physics, (CRC Press. Boca Raton 2003).

10. A. Seaton, L. Yin, R. Follett, B. Albright and A. Le, 2022, "Cross-beam energy transfer in direct-drive ICF. I. Nonlinear and kinetic effects," Physics of Plasmas, 29(4) 042706. doi: 10.1063/5.0078800

11. C. Garban-Labaune, E. Fabre, C. E. Max, R. Fabbro, F. Amiranoff, J. Virmont, M. Weinfeld and A. Michard, 1982, "Effect of Laser Wavelength and Pulse Duration on Laser-Light Absorption and Back Reflection," Physics Review Letters, 48(15) 1018-1021. doi: 10.1103/PhysRevLett.48.1018

12. R. Lehmberg and S. Obenschain, 1983, "Use of induced spatial incoherence for uniform illumination of laser fusion targets," Optics Communications, 46(1), 27-31. doi: 10.1016/0030-4018(83)90024-X

13. S. Skupsky, R. W. Short, T. Kessler, R. S. Craxton, S. Letzring and J. M. Soures, 1989, "Improved laser-beam uniformity using the angular dispersion of frequency-modulated light," Journal of Applied Physics, 66(8), 3456-3462. doi: 10.1063/1.344101

14. J. Thomson, 1975 "Finite-bandwidth effects on the parametric instability in an inhomogeneous plasma," Nucl. Fusion, 15(2), 237-247. doi: 10.1088/0029-5515/15/2/008

15. C.Rousseaux, S.D. Baton, D. Benisti, L.Gremillet, B.Loupias, F.Philippe, V.Tassin, F.Amiranoff, J.L.Kline, D.S.Montgomery, B.B.Afeyan, 2016, " Experimental investigation of stimulated Raman and Brillouin scattering instabilities driven by two successive collinear picosecond laser pulses," Physical Review E 93, 043209. doi: 10.1103/PhysRevE.93.043209

16. G. Bonnaud and C. Reisse, 1986, "Particle code study of the influence of non-monochromaticity of laser light on stimulated Raman scattering in laser-irradiated plasmas," Nuclear Fusion, 26(5) 633-646. doi: 10.1088/0029-5515/26/5/008

17. H. Zhou, C. Xiao, D. Zou, X. Li, Y. Yin, F. Shao and H. Zhuo, 2018 "Numerical study of bandwidth effect on stimulated Raman backscattering in nonlinear regime," Physics of Plasmas, 25(6), 062703. doi: 10.1063/1.5030153

18. W. Kaiser, "Stimulated Rayleigh, Brillouin and Raman spectroscopy," in Laser Handbook, 2 ed., North-Holland, 1972, pp. 1077-1150.

19. V. S. Averbakh, A. I. Makarov and V. I. Talanov, 1978, "Stimulated Raman scattering on rotational and vibrational transitions in nitrogen gas," Soviet Journal of Quantum Electronics, 8(4), 472-476. doi: 10.1070/QE1978v008n04ABEH010057

20. M. Rokni and A. Flusberg, 1986, "Stimulated Rotational Raman Scattering in the Atmosphere," IEEE Journal of Quantum Electronics, QE-22(7), 1102-1108. doi: 10.1109/JQE.1986.1073083

21. M. A. Henesian, C. D. Swift and J. R. Murray, 1985 "Stimulated rotational Raman scattering in nitrogen in long air paths," Optics letters, 10(11), 565-567. doi: 10.1364/OL.10.000565

22. Y. Lin, T.J. Kessler, G.N. Lawrence, 1994, "Raman scattering in air: Four-dimensional analysis," Applied Optics 33(21) 4781-4791. doi: 10.1364/AO.33.004781

23. J. Bates, R. Follett, J. Shaw, S. M. J. Obenschain, J. Weaver, M. Wolford, D. Kehne, M. Myers and T. Kessler, 2023, "Suppressing parametric instabilities in direct-drive inertial-confinement-fusion plasmas using broadband laser light," Physics of Plasmas, vol. 30, no. 5, 2023. doi: 10.1063/5.0150865

24. J. Weaver, R. Lehmberg, S. Obenschain, D. Kehne, M. Wolford, 2017, "Spectral and far-field broadening due to stimulated rotational Raman scattering driven by the Nike krypton fluoride laser," Applied Optics 56(31), 8618-8631. doi: 10.1364/AO.56.008618

25. D. M. Kehne and J. L. Weaver, U.S. Naval Research Laboratory, private communication, 2022.

26. S.A. McLaren, S. Schrauth, K. McCandless, J. Penner, R. Aden, J.M. Di Nicola, 2023, "Four-dimensional dynamics of multirotational transition stimulated rotational Raman scattering in air," Journal of the Optical Society of America B 40(7) 1800-1805. doi: 10.1364/JOSAB.490088

27. S. Gao, Y. Wang, F. Belli, C. Brahms, P. Wang and J. Travers, 2022, "From Raman Frequency Combs to Supercontinuum Generation in Nitrogen-Filled Hollow-Core Anti-Resonant Fiber," Laser & Photonics Reviews, 6(4) 2100426. doi: 10.1063/5.0150865

28. Continuum Laser Manual for Project #17/14979 at NRL.

29. T.J. Kessler, Y. Aglitskiy, M. Karasik, S. Velikovich, 2023, "Laser Machining of Sinusoidal Perturbation," NRL Memorandum NRL/6730/MR—2023/2

30. M.F. Wolford, M.C. Myers, F. Hegeler, J.D. Sethian, 2016, "Dynamics of Laser Triggered, Gas-Insulated Spark Gaps During Repetitive Operation," IEEE Transactions of Plasma Science 44(10) 2410-2423. doi: 10.1109/TPS.2016.2606249

31. R.J. Butcher, D.V. Willetts, W.J. Jones, 1971, "On the Use of Fabry-Perot Etalon for the Determination of Rotational Constants of Simple Molecules-The Pure Rotational Raman Spectra of

Oxygen and Nitrogen," Proceedings of the Royal Society of London, Series A, Mathematical and Physical Sciences, 324(1557) 231-245.

32. V.S. Averbakh, A.I. Makarov, V.I. Talanov, 1978, "Stimulated Raman scattering on rotational and vibrational transitions in nitrogen gas," Sov. J. Quantum Electron. 8 472-476.

33. S. Dixit, M. Hermann, T. Karr, 1989, "High Intensity Effects in Raman Scattering," In Eberly, J.H., Mandel, L. Wolf, E. (eds) Coherence and Quantum Optics VI, Springer, Boston, MA. 227-236. doi: 10.1007/978-1-4613-0847-8_43

34. V.I. Talanov, 1970, "About Self-Focusing of Light in Cubic Media," JETP Lett. 11 199-201.

35. R.H. Lehmberg, 2017 private communication.

36. E.A. Sziklas, A.E. Siegman, 1975, "Mode Calculations in unstable resonators with flowing saturable gain. 2: Fast Fourier transform method," Applied Optics 14(8) 1874-1889. doi: 10.1364/AO.14.001874

37. B.R. Suydam, 1974, "Self-focusing of very powerful laser beams II," IEEE Journal of Quantum Electronics 10(11) 837-843. doi: 10.1109/JQE.1974.1068106

38. J.H. Marburger, 1975, "Self-focusing: Theory," Progress in Quantum Electronics 4 35-110. doi: 10.1016/0079-6727(75)90003-8

39. M.D. Duncan, R. Mahon, J. Reintjes, LL. Tankersley, 1986, "Parametric Raman gain suppression in D_2 and H_2," Optic Letters 11, 803-805. doi: 10.1364/OL.11.000803

40. M.A. Henesian, D.M. Pennington, 1986, "Observation of parametric gain suppression in stimulated rotational Raman scattering over long air paths," in Conference on Lasers and Electro-Optics (CLEO), Anaheim, CA, 25-29 April, paper WN1.

41. K. Leung, M. Oron, D. Klemek, R. Holmes, A. Flusberg, 1988, "Observation of parametric gain suppression in rotational Raman transitions of N_2 and H_2," Optics Letters 13(1) 33-35. doi: 10.1364/OL.13.000033

42. P. E. Ciddor, 1996, "Refractive index of air: new equations for the visible and near infrared," Applied Optics 35(9) 1566-1573. doi: 10.1364/AO.35.001566

43. D.M. Pennington, M.A. Henesian, R.W. Hellwarth, 1989, "Nonlinear index of air at 1.053 μm," Phys. Rev. A. 39 3003-3009. doi: 10.1103/PhysRevA.39.3003

44. Yu.E. Geints, A.M. Kabanov, A.A. Zemlyanov, E.E. Bykova, O.A. Bukin, S.S. Golik, 2011, "Kerr-driven nonlinear refractive index of air at 800 and 400 nm measured through femtosecond laser pulse filamentation," Applied Physics Letters 99 181114. doi: 10.1063/1.3657774

45. S. Zahedpour, J.K. Wahlstrand, H.M. Milchberg, 2015, "Measurement of the nonlinear refractive index of air constituents at mid-infrared wavelengths," Optics Letters 40(24) 5794-5797. doi: 10.1364/OL.40.005794

46. Estimates utilized for present calculations

47. S.V. Mel'chenko, 1991, "Efficient conversion by stimulated Raman scattering of the radiation of a XeCl laser into the anti-Stokes region," Soviet Technical Physics Letters 17(2) 120-121.

48. M.A. Henesian, C.D. Swift, J.R. Murray, 1985, "Stimulated rotational Raman scattering in nitrogen in long air paths," Optics Letters 10(11) 565-567. doi: 10.1364/OL.10.000565

49. M.A. Henesian, D.M. Pennington, 1988, "Diffraction Properties Of Laser Speckle Generated By Stimulated Rotational Raman Scattering in Long Air Paths," Proc. SPIE 0874, Nonlinear Optical Beam Manipulation, Beam Combining, and Atmospheric Propagation, (8 April 1988); doi: 10.1117/12.943798

50. S.A. McLaren, S. Schrauth, K. McCandless, J. Penner, R. Aden, J.M. DiNicola, 2023, "Four-dimensional dynamics of multirotational transition stimulated rotational Raman scattering in air," Journal of the Optical Society of America B 40(7) 1800-1806. doi: 10.1364/JOSAB.490088

51. J.W. Bates, R.K. Follett, J.G. Shaw, S.P. Obenschain, R.H. Lehmberg, J.F. Myatt, J.L. Weaver, D.M. Kehne, M.F. Wolford, M.C. Myers, T.J. Kessler, 2020, "Suppressing cross-beam energy transfer with broadband lasers," High Energy Density Physics 36, 100772. doi: 10.1016/j.hedp/2020.100772

52. J.W. Bates, J.F. Myatt, J.G. Shaw, R.K. Follett, J.L. Weaver, R.H. Lehmberg, S.P. Obenschain, 2018 "Mitigation of cross-beam energy transfer in inertial-confinement-fusion plasmas with enhanced laser bandwidth," Physical Review E 97, 061202. doi: 10.1103/PhysRevE.97.061202

53. D. Eimerl, W.L. Kruer, E.M. Campbell, 1992, "Ultrabroad bandwidth for suppression of laser driven parametric instabilities," Comments Plasma Phys. Controlled Fusion 15(2) 85-104.

54. J. Bates, J. Myatt, J. Shaw, R. Follett, J. Weaver, R. Lehmberg, S. Obenschain, 2018, "Mitigating cross-beam energy transfer in directly-driven inertial confinement-fusion targets using broadband laser light," APS Division of Plasma Physics Meeting 2018

55. Z. Epstein, R.H. Lehmberg, P. Sprangle, 2019, "Spectral Broadening of a KrF laser via propagation through Xe in the negative nonlinear index regime," Physical Review A. 100 023831. doi: 10.1103/PhysRevA.100.023831

56. K.A. Stankov, Y.-W. Lee, 1992, "Efficient Raman Conversion of Femtosecond UV light pulses," Ultrafast Phenomena VIII Eds: J.-L. Martin, A. Migus, G.A. Mourou, A.H. Zewail, 311-312.

ACKNOWLEDGEMENTS

We would like to thank the financial support of Department of Energy/NNSA. We would also like to thank Dr. Jason Bates, Dr. James Weaver and Dr. David Kehne for helpful scientific discussions. We would like to thank Matt Myers, Areg Mangassarian, Dr. Lop-Yung Chan and Laodice Granger for logistics in the laboratory in setting up the experiment. We greatly appreciate the inordinate amount of support and assistance from our deceased former colleagues Dr. Robert H. Lehmberg and Dr. David Eimerl. We would like to thank Hubert Jean-Ruel, Taylor Breen, and Greg Wardle of Lightmachinery for providing custom software and support fine-tuning the Hyperfine spectrometer. We would like to thank the David Parrino of Stellarnet for helpful spectrometer implementation discussions. We would like to thank Glen Dong and Dr. James Norby of Amplitude Laser for providing their expertise and support with regard to the 10J ND:Glass green laser system.